

**RIVULET FLOWS AND FLOWS AROUND DRY
PATCHES ON AN INCLINED PLANE**

NURUL AININA BINTI REDWAN

UNIVERSITI SAINS MALAYSIA

2021

**RIVULET FLOWS AND FLOWS AROUND DRY
PATCHES ON AN INCLINED PLANE**

by

NURUL AININA BINTI REDWAN

**Thesis submitted in fulfilment of the requirements
for the degree of
Doctor of Philosophy**

November 2021

ACKNOWLEDGEMENT

Alhamdulillah - All praises and thanks to Allah, The Almighty, The All-Knowing, The Most Merciful for granting me courage and strength to accomplish this thesis.

My utmost respect and heartfelt gratefulness for my supervisor, Dr Yazariah Mohd Yatim for her never-ending guidance, encouragement, tireless supervision and such patience for this unexpectedly long but yet enriching experience. May Allah shower His constant blessings on you and your beloved ones in return.

I am profoundly grateful to Prof. Stephen Wilson and Dr Brian Duffy for their constructive ideas and suggestions in my research. My sincere appreciation to Prof. Hailiza Kamarulhaili, Assoc. Prof. Dr Farah Aini Abdullah and Prof. Jamaludin Ali for encouraging me to pursue my studies.

This work is dedicated to my dear parents, Shabariah Ahmed and Redwan Adnan and to my brother Amir Izat Redwan for their patience, support, love and unflagging belief throughout my life.

I would like to convey my appreciation to my friends for their insightful comments, invaluable discussions, emotional support, comedic relief and cheer me up with food to keep me stay in the groove. I also would like to express my gratitude to the staffs of the School of Mathematical Sciences and Institute of Postgraduate Studies USM for their helps on technical matters. I am indebted for their time and effort.

Last but not least, this thesis would have not been accomplished with the support from MyBrain15 for personal financial assistance during my study. Not to forget, School of Mathematical Sciences for research facilities, workshops and conferences sponsorship.

TABLE OF CONTENTS

ACKNOWLEDGEMENT	ii
TABLE OF CONTENTS	iii
LIST OF TABLE	vii
LIST OF FIGURES	viii
LIST OF SYMBOLS	xiii
ABSTRAK	xix
ABSTRACT	xxi
CHAPTER 1 INTRODUCTION	1
1.1 Overview of Thin-Film Flow	1
1.2 Rivulet and Dry Patch	4
1.3 Classification of Fluids	7
1.3.1 Newtonian Fluid	8
1.3.2 Non-Newtonian Fluid	8
1.3.3 Power-Law Fluid Model	11
1.4 Significance of Strong Surface-Tension Effect	13
1.5 Motivations of Study	15
1.6 Problem Statement	19
1.7 Aim and Objectives of Study	21
1.8 Limitation of Study	22
1.9 Research Methodology	23
1.10 Thesis Outline	24

CHAPTER 2 LITERATURE REVIEW	27
2.1 A Brief History of the Navier-Stokes Equation	27
2.2 Thin-Film Fluid Flows Driven by External Forces	33
2.2.1 Rivulet Flow	33
2.2.2 Flow Around a Dry Patch.....	49
2.3 Thin-Film Fluid Driven by Other Mechanisms	59
2.4 Conclusion	63
CHAPTER 3 METHODOLOGY.....	64
3.1 Governing Equations	65
3.1.1 A Newtonian Fluid	65
3.1.2 Power-Law Fluid Model	67
3.2 The Lubrication Approximation	68
3.3 Mathematical Modelling of Thin-Film Flow	70
3.3.1 Two-Dimensional Thin-Film Flow of a Newtonian Fluid.....	70
3.3.2 Three-Dimensional Thin-Film Flow of a Power-Law Fluid	72
3.4 Boundary Conditions	75
3.4.1 Two-Dimensional Thin-Film Flow of a Newtonian Fluid.....	77
3.4.2 Three-Dimensional Thin-Film Flow of a Power-Law Fluid	80
3.5 Similarity Solution	91
3.6 Numerical Method: Shooting Method.....	93
CHAPTER 4 UNSTEADY GRAVITY-DRIVEN RIVULET FLOW OF NEWTONIAN AND NON-NEWTONIAN POWER-LAW FLUIDS WITH STRONG SURFACE-TENSION EFFECT ..	99
4.1 Problem Formulation	100
4.2 Results and Discussions	108

4.3	Conclusions	122
CHAPTER 5 UNSTEADY GRAVITY-DRIVEN FLOW OF NEWTONIAN AND NON-NEWTONIAN POWER-LAW FLUIDS AROUND A DRY PATCH WITH STRONG SURFACE-TENSION EFFECT		
5.1	Problem Formulation	124
5.2	Results and Discussions	129
5.3	Conclusions	139
CHAPTER 6 UNSTEADY SHEAR-STRESS-DRIVEN RIVULET FLOWS OF NEWTONIAN AND NON-NEWTONIAN POWER-LAW FLUIDS WITH STRONG SURFACE-TENSION EFFECT		
6.1	Problem Formulation	141
6.2	Results and Discussions	149
6.3	Conclusions	161
CHAPTER 7 UNSTEADY SHEAR-STRESS-DRIVEN FLOW OF NEWTONIAN AND NON-NEWTONIAN POWER-LAW FLUIDS AROUND A DRY PATCH WITH STRONG SURFACE-TENSION EFFECT		
7.1	Problem Formulation	162
7.2	Results and Discussions	166
7.3	Conclusions	174
CHAPTER 8 STEADY RIVULET FLOW OF PERFECTLY WETTING NEWTONIAN FLUID WITH THERMOCAPILLARY EFFECT		
8.1	Problem Formulation	176
	8.1.1 The Transverse Flow	186
8.2	Results and Discussions	188
8.3	Conclusions	195
CHAPTER 9 CONCLUSIONS AND FUTURE WORK		
		196

9.1	Conclusions	196
9.2	Suggestions for Future Work.....	200
	REFERENCES	202

APPENDICES

LIST OF PUBLICATIONS

LIST OF TABLE

	Page
Table 3.1 Algorithm of the shooting method for non-linear problem (3.127).....	97

LIST OF FIGURES

		Page
Figure 1.1	(a) Brick with guilloché design. (Source picture: https://www.metmuseum.org/art/collection/search/324618). (b) A gateway to Emirates Stadium. (Source picture: https://ibstockbrick.co.uk/news/a-striking-gateway-to-emirates-stadium/).....	3
Figure 1.2	Formation of rivulets, dry patches and droplets.	5
Figure 1.3	Sketch of a simple shearing flow.	7
Figure 1.4	The relationship between the shear stress, τ and shear rate, $\dot{\gamma}$ for Newtonian and certain generalised Newtonian fluids (time-independent fluids).....	9
Figure 1.5	Water striders on surface of water. (Source picture: https://www.pestwiki.com/water-strider-facts-rid/)	14
Figure 1.6	A droplet and air bubble in outer space. (Source picture: https://www.nasa.gov/audience/forstudents/5-8/features/space_gardens_feature.html).....	15
Figure 1.7	Rivulet flows on an inclined plane.	18
Figure 1.8	The flow chart of research methodology.....	26
Figure 2.1	Three-dimensional plot of similarity solution by Smith (1973)...	35
Figure 2.2	Three-dimensional plot of a widening rivulet at cooled substrate due to thermocapillarity for (a) gravity-driven and (b) shear-stress-driven. Reprinted from Holland et al. (2003) with permission of Oxford University Press.	36
Figure 2.3	Flow of different fluid with different surface tension on an inclined plane. (a) Silicone oil (b) Glycerine. Reprinted from Huppert (1982a) with permission of Nature.....	37
Figure 2.4	Three-dimensional plot of sessile rivulets (a) and (b) gravity-driven, and (c) shear-stress-driven at different times. Reprinted from Yatim et al. (2011) with permission of Oxford University Press. Reprinted from Yatim et al. (2012) with permission of Springer Nature.	41

Figure 2.5	Streamline of the transverse flow when the substrate is colder than the environment. Reprinted from Holland et al. (2001) with permission of Cambridge University Press.	44
Figure 2.6	Contour plot of the velocity when large Navier slip. Reproduced from Alshaikhi et al. (2020), with the permission of AIP Publishing.....	46
Figure 2.7	Formation of rivulets and dry patches. (a) Dry zone. (b) Downward moving arch. The inset shows the rim around the dry patch. Reproduced from Podgorski et al. (1999), with the permission of AIP Publishing.....	53
Figure 2.8	Three-dimensional plot of dry patch down an inclined plane at $t = 6$. Picture courtesy of Abas (2017).	56
Figure 2.9	Evolution of hole shape in time, s from top view on (a) silanised aluminium substrate and (b) silicone substrate. Reprinted from Lv et al. (2018)) with permission of Cambridge University Press.	58
Figure 2.10	Measuring the height profile near the front using the laser line in experiment. Reprinted from Mavromoustaki et al. (2018), Surface tension effects for particle settling and resuspension in viscous thin films, Nonlinearity, 31 , 3151, 25 May 2018. © IOP Publishing Ltd & London Mathematical Society. Reproduced by permission of IOP Publishing. All rights reserved.	62
Figure 3.1	Sketch of the geometry for unsteady two-dimensional thin-film flow down an inclined plane.	69
Figure 3.2	Sketch of the geometry for unsteady three-dimensional thin-film flow down an inclined plane.	73
Figure 3.3	Cross-sectional profile of a symmetric rivulet when $H_2 = -1$	93
Figure 3.4	Shooting method for non-linear problems (Burden and Faires, 2010).	95
Figure 3.5	Shooting method for a rivulet problem.	97
Figure 3.6	Shooting method for a dry patch problem.	98
Figure 4.1	Plot of η_0 as a function of H_0 for variation of N when (a) $H_2 = -1$, (b) $H_2 = 0$ and (c) $H_2 = 1$. The Newtonian fluid, $N = 1$ is denoted with a dashed line.	115

Figure 4.2	Plot of C as a function of H_0 for variation of N when (a) $H_2 = -1$, (b) $H_2 = 0$ and (c) $H_2 = 1$. The insets show the enlargement of H_{0c} curves.	116
Figure 4.3	Plot of $I(=J)$ as a function of N for $H_0 = H_{0c}$ when $H_2 = -1$ and $H_2 = 0$	117
Figure 4.4	The cross-sectional profiles $H = H(\eta)$ for $H_0 = H_{0c}$ with variation of N when (a) $H_2 = -1$ and (b) $H_2 = 0$. The Newtonian fluid, $N = 1$ is denoted with a dashed line.	118
Figure 4.5	Three-dimensional plots for (a) $H_2 = -1$ ($H_{0c} \simeq 1.1199$) and (b) $H_2 = 0$ ($H_{0c} \simeq 1.0548$) at times $t = 1, 10$ and 100 when $N = 1/5$	119
Figure 4.6	Three-dimensional plots for (a) $H_2 = -1$ ($H_{0c} \simeq 1.2004$) and (b) $H_2 = 0$ ($H_{0c} \simeq 1.0949$) at times $t = 1, 10$ and 100 when $N = 1$	120
Figure 4.7	Three-dimensional plots for (a) $H_2 = -1$ ($H_{0c} \simeq 1.2418$) and (b) $H_2 = 0$ ($H_{0c} \simeq 1.1157$) at times $t = 1, 3$ and 5 when $N = 20$	121
Figure 5.1	Sketch of the geometry of three-dimensional unsteady thin-film flow down an inclined plane.	125
Figure 5.2	The cross-sectional profile of dry patch with capillary ridge.	127
Figure 5.3	The cross-sectional profiles $H(\eta)$ plotted as a function of η when $\phi = 0$ and $N = 1$ for $A = -60, -50, -40, -30, -20$ and A_c in (a) Case 1 ($S_t = +1$) and, for $A = -5, -4, -3, -2, -1$ and A_c in (b) Case 2 ($S_t = -1$).	133
Figure 5.4	The cross-sectional profiles $H(\eta)$ in Case 1 ($S_t = +1$) plotted as a function of η when $N = 1$ and $A = -60$ for $\phi = 0, \pi/16, \pi/8, 3\pi/16, \pi/4$ and $5\pi/16$	134
Figure 5.5	The cross-sectional profiles $H(\eta)$ plotted as a function of η when $\phi = 0$ and $A = -60$ for $N = 1/5, 1/2, 1, 2$, and 5 in (a) Case 1 ($S_t = +1$) and (b) Case 2 ($S_t = -1$).	136
Figure 5.6	Three-dimensional plots for Case 1, $A = -60, N = 1/2, 1$ and 2 when (a) $t = 1$, (b) $t = 5$ and (c) $t = 10$ (from left to right).	137
Figure 5.7	Three-dimensional plots for Case 2, $A = -60, N = 1/2, 1$ and 2 when (a) $t = -1$, (b) $t = -5$ and (c) $t = -10$ (from left to right).	138

Figure 6.1	Sketch of the geometry of three-dimensional unsteady thin-film flow down an inclined plane driven by constant shear stress, τ at the free surface.	142
Figure 6.2	Plot of η_0 as a function of H_0 for (a) $H_2 \leq 0$ and (b) $H_2 > 0$	153
Figure 6.3	Plot of η_0 as a function of H_2 for $H_0 = 20, 40, 60, 80$ and 100 . ..	154
Figure 6.4	The cross-sectional profiles $H = H(\eta)$ for a range of values of H_0 when (a) $H_2 = -1$, (b) $H_2 = 0$ and (c) $H_2 = 0.8$	156
Figure 6.5	Plot of I_1 as function of H_0 for (a) $H_2 = -1000, -100, -10, -1$ and 0 , and (b) $0.2, 0.4$ and 0.6	157
Figure 6.6	Plot of I_2 as function of H_0 for (a) $H_2 = -1000, -100, -10, -1$ and 0 , and (b) $H_2 = 0.2, 0.4$ and 0.6	158
Figure 6.7	Plot of C given by (6.42) as a function of H_0 for (a) $H_2 \leq 0$ and (b) $H_2 > 0$	159
Figure 6.8	Three-dimensional plots for (a) $H_2 < -1$ ($H_{0c} \simeq 1.3635$) and (b) $H_2 = -1$ ($H_{0c} \simeq 1.3536$) and (c) $H_2 = 0$ ($H_{0c} \simeq 1.2121$) at times $t = 1, 10$ and 100 in Case 1.	160
Figure 7.1	Sketch of the geometry of the three-dimensional unsteady thin-film flow down an inclined plane driven by constant shear stress, τ at the free surface.	163
Figure 7.2	The cross-sectional profiles $H(\eta)$ plotted as a function of η when $\phi = 0$ for $A = -80, -70, -60 - 50, -40, -30$ and A_c in (a) Case 1 ($S_t = +1$), and for $A = -A_{c1}, -2, -1.5 - 1, -0.5$ and A_c in (b) Case 2 ($S_t = -1$).	168
Figure 7.3	The cross-sectional profiles $H(\eta)$ in Case 1 ($S_t = +1$) plotted as a function of η when $A = -60$ for $\phi = 0, \pi/6, \pi/8, 3\pi/16, \pi/4$ and $5\pi/16$	169
Figure 7.4	Three-dimensional plots for Case 1 and $A = -60$ when (a) $t = 1$, (b) $t = 5$ and (c) $t = 10$	172
Figure 7.5	Three-dimensional plots for Case 2 and $A = -1$ when (a) $t = -1$, (b) $t = -5$ and (c) $t = -10$	173
Figure 8.1	Geometry of the problem in xz - and yz - planes.	177
Figure 8.2	Numerically calculated solutions for (a) h_m and (b) a , plotted as functions of α/π for $Q = 0.1, 1, 10, 100$ and 1000 when $M = 1$	191

Figure 8.3	Numerically calculated solutions for (a) h_m and (b) a , plotted as functions of α/π for $M = 1, 10, 100$ and 1000 when $Q = 1$	192
Figure 8.4	Transverse profile for (a) $0 < \alpha < \pi/2$ (sessile rivulet) and (b) $\pi/2 < \alpha < \pi$ (pendent rivulet) when $Q = M = 1$	193
Figure 8.5	Streamlines of the transverse flow at vertical substrate $\alpha = \frac{1}{2}\pi$ in the cases (a) $Q = 1, M = 0.01$, and (b) $Q = 1, M = 3$. The curves $z = \frac{2}{3}h$ (which the streamlines cross ‘vertically’) are also shown.	194
Figure D.1	<i>Mathematica</i> coding for rivulet problem (Case 1): Solve (3.124) subject to the conditions (3.125) for H when $N = 1$ using <code>NDSolve</code> , and plot the cross-sectional profile.	228
Figure D.2	<i>Mathematica</i> coding for dry patch problem (Case 1): Solve for (3.124) subject to the conditions (5.19) for H when $N = 1$ using <code>NDSolve</code> , and plot the cross-sectional profile.	229

LIST OF SYMBOLS

Roman Letters

a	semi-width of the rivulet/dry patch
A	constant in the dry patch solution
A_r	cross-sectional area difference
A_0	area of a finite length
A_c	critical value of the rivulet/dry patch
ΔA	cross-sectional area of the dry patch
b	constant in the similarity solution
B	constant in the dry patch solution
B	Biot number
B_r	real constant in the dry patch solution
B_i	complex constant in the dry patch solution
c	constant in the similarity solution
c_p	specific heat
C	constant
C_i	constant of integration, $i = 1, 2, 3, 4, 5$
Ca	capillary number
ΔC	thermocapillary number
d	constant in the similarity solution

e	exponent in the similarity solution
f	exponent in the similarity solution
F	functional of η
g	gravitational acceleration
G_1	constant of the total volume flux in the dry patch
h	fluid thickness
h_∞	uniform fluid thickness
h_m	middle height
h_{\max}	capillary ridge height
h_s	stagnation point height
H	functional of η
H_0	free parameter in the middle height
H_{0c}	critical free parameter in the middle height
H_2	free parameter in the middle height
H_{\max}	non-dimensional maximum height of the rivulet/dry patch
H_∞	non-dimensional height far from the dry patch
i	iteration of the shooting method
I	constant of the cross-sectional area
j	iteration of the shooting method
J	constant of the volume flux
k	constant in the similarity solution

k_{th}	thermal conductivity
K	consistency parameter of fluid
K_i	constant in the behaviour near $\eta = \eta_0$, $i = 1, 2, 3$
ℓ	exponent in the similarity solution
L	typical fluid length
L_0	finite length
m	mass of a particle
m	exponent in the behaviour near $\eta = \eta_0$
M	maximum number of iteration
M	Marangoni number
n	exponent in the similarity solution
\bar{n}	interval of the shooting method
\bar{n}_0	initial point of the shooting method
\bar{n}_∞	end point of the shooting method
N	power-law index
O	origin in a Cartesian coordinate system
p	pressure of the fluid
p_a	atmospheric pressure
p_∞	uniform fluid pressure
Q	volume flux
ΔQ	cross-sectional volume difference

r	exponent in the similarity solution
R	exponent in the behaviour near $\eta = \eta_0$
s	exponent in the similarity solution
S	constant in the dry patch solution
t	time variable
T	temperature of the fluid
T_0	prescribed uniform temperature of the substrate
T_∞	prescribed uniform temperature of the passive atmosphere
\bar{T}	time scale
u	fluid velocity in the x -direction
u_∞	uniform fluid velocity in the x -direction
\bar{u}	local flux in the x -direction
U	depth-averaged velocity
v	fluid velocity in the y -direction
\bar{v}	local flux in the y -direction
V	plate velocity
w	fluid velocity in the z -direction
x	longitudinal direction to the plane
\bar{X}	length scale
y	transverse direction to the plane
Y	constant in the dry patch solution

z	normal direction to the plane
Z	constant in the dry patch solution

Greek Letters

α	angle of the inclination
α_{th}	unit surface thermal conductance
δ	non-dimensional longitudinal aspect ratio
ε	non-dimensional transverse aspect ratio
η	non-dimensional similarity variable
η_0	non-dimensional semi-width of the rivulet/dry patch
η_{0c}	non-dimensional critical semi-width of the rivulet/dry patch
γ	shear rate of the fluid
κ	mean curvature of the free surface
λ	constant of surface tension varies on temperature
μ	apparent viscosity of the fluid
μ_0	consistency coefficient of the fluid
ϕ	phase shift
ρ	density of the fluid
σ	surface tension of the fluid
σ_0	constant surface tension
τ	shear stress of the fluid
τ_0	yield shear stress

ϑ power of the concentration

ζ number of dimension

Superscripts

' differentiation with respect to η

* non-dimensional variables

ALIRAN JEJURUS DAN ALIRAN DI SEKITAR TOMPOK KERING DI ATAS SATAH CONDONG

ABSTRAK

Aliran filem nipis telah menarik perhatian para penyelidik daripada pelbagai bidang seperti biologi, geofizik dan industri. Tesis ini membentangkan kajian bagi aliran filem nipis untuk bendalir Newtonan dan bendalir hukum kuasa bukan Newtonan di atas satah condong. Khususnya, aliran bagi jejurus yang lampai dan aliran di sekitar tompok kering yang lampai dipertimbangkan. Aliran bendalir didorong oleh graviti atau tegasan ricih pada permukaan bebas dengan kesan tegangan permukaan yang kuat. Penghampiran pelinciran digunakan pada persamaan keselajaran dan persamaan Navier-Stokes. Persamaan-persamaan ini yang tertakluk kepada syarat sempadan tanpa gelincir dan tiada penembusan, keseimbangan tegasan normal dan tangen beserta syarat kinematik menghasilkan persamaan pembezaan separa menakluk peringkat keempat. Untuk menurunkan persamaan pembezaan separa kepada persamaan pembezaan biasa, penjelmaan keserupaan digunakan. Kemudian, persamaan pembezaan biasa dijadikan tak berdimensi dengan menggunakan pemboleh ubah tak berdimensi. Akhirnya, persamaan ini diselesaikan menggunakan kaedah tembakan melalui perisian *Mathematica* 12. Satu penyelesaian keserupaan yang realistik diperoleh bagi aliran jejurus dengan profil keratan rentas berbonggol tunggal. Manakala, dua penyelesaian keserupaan yang realistik diperoleh bagi aliran di sekitar tompok kering iaitu, satu penyelesaian dengan profil keratan rentas yang meningkat secara monotonik dan satu lagi ialah penyelesaian dengan profil keratan rentas yang meningkat secara berayun. Penyelesaian keserupaan aliran yang didorong oleh graviti menunjukkan bahawa pada

bila-bila masa t , aliran jejurus dan tompok kering melebar dengan $|x|^{(2N+1)/4(N+1)}$ dan menebal dengan $|x|^{N/(N+1)}$. Penyelesaian keserupaan juga menunjukkan bahawa pada mana-mana stesen x , aliran jejurus dan tompok kering mengecil dengan $|t|^{-N/4(N+1)}$ dan menipis dengan $|t|^{-N/(N+1)}$, dengan N ialah indeks hukum kuasa bendalir bukan Newtonan. Sementara itu, bagi aliran yang didorong oleh tegasan ricih, penyelesaian keserupaan yang didapati menunjukkan bahawa pada bila-bila masa t , aliran jejurus dan tompok kering melebar dengan $|x|^{3/4}$ dan menebal dengan $|x|$, dan pada mana-mana stesen x , aliran jejurus dan tompok kering mengecil dengan $|t|^{-1/2}$ dan menipis dengan $|t|^{-1}$. Untuk aliran jenis ini, penyelesaian keserupaan yang didapati tidak bergantung kepada N , berbeza dengan aliran yang didorong oleh graviti. Walaupun daya fizikal berbeza digunakan bagi memandu aliran pada permukaan bebas seperti graviti dan tegasan ricih, penyelesaian untuk aliran jejurus dan aliran di sekitar tompok kering adalah didapati serupa secara kualitatif pada profil keratan rentas. Peranan kesan tegangan permukaan yang kuat banyak ditemui dalam kajian proses penghabluran seperti hablur protein dalam penghasilan ubatan baru. Tesis ini turut mengkaji aliran jejurus tak isoterma bagi bendalir Newtonan pembasahan sempurna di atas substrat satah condong. Substrat tersebut sama ada bersuhu lebih panas secara seragam (dengan nombor Marangoni $M > 0$) atau lebih sejuk secara seragam (dengan $M < 0$) berbanding dengan suhu persekitaran. Perbezaan suhu antara substrat dan persekitaran menghasilkan perubahan ketegangan permukaan di permukaan bebas bendalir. Penyelesaian boleh didapati untuk semua sudut kecondongan satah α apabila $M > 0$. Namun begitu, apabila $M < 0$, tiada penyelesaian diperolehi untuk kes ini. Pembasahan sempurna sangat penting dalam pengeluaran salut berkualiti tinggi untuk mengelakkan pengakisan.

RIVULET FLOWS AND FLOWS AROUND DRY PATCHES ON AN INCLINED PLANE

ABSTRACT

Thin-film flow has gained interest among researchers from different fields such as biology, geophysics and industry. This thesis presents a study on the thin-film flows of Newtonian and non-Newtonian power-law fluids on an inclined plane. Specifically, flow of slender rivulet and flow around slender dry patch are considered. The gravity or shear stress at the free surface drives the flow in the case of strong surface-tension effects. The lubrication approximation is applied to the continuity equation and Navier-Stokes equations. These equations are subject to the boundary conditions of no-slip and no-penetration, the balances of normal and tangential stress together with the kinematic condition to yield a fourth-order governing partial differential equation. To reduce the governing partial differential equation to the ordinary differential equation, the similarity transformation method is used. Then, the latter equation is non-dimensionalised by using non-dimensional variables. Finally, the governing equation is solved using a shooting method via *Mathematica* 12 software. A physically realisable similarity solution is obtained for rivulet flow with a single-humped cross-sectional profile. Meanwhile, there are two distinct physically realisable similarity solutions are obtained for dry patches, one with monotonically-increased cross-sectional profile and another one, with a cross-sectional profile that increases in an oscillatory manner. The similarity solution of the flow driven by gravity predicts that at any time t , the rivulet and the dry patch widen according to $|x|^{(2N+1)/4(N+1)}$ and thicken according to $|x|^{N/(N+1)}$. The similarity solution also shows that at any station x , the rivulet

and the dry patch narrow according to $|t|^{-N/4(N+1)}$ and thin according to $|t|^{-N/(N+1)}$, where N is the power-law index of non-Newtonian fluid. Meanwhile, for the flow driven by shear stress, the similarity solution shows that at any time t , the rivulet and the dry patch widen according to $|x|^{3/4}$ and thicken according to $|x|$, and that at any station x , the rivulet and the dry patch narrow according to $|t|^{-1/2}$ and thin according to $|t|^{-1}$. For the flow driven by shear stress, the similarity solution obtained does not depend on N , which is different from the flow driven by gravity. Regardless of different physical forces such as gravity and shear stress that driving the flow on the free surface, the solutions for rivulet and dry patch flows are qualitatively similar in the cross-sectional profiles. The role of strong surface-tension effect is preferred in crystallisation development research such as protein crystal in producing new medicine. This thesis also presents non-isothermal rivulet flow of perfectly wetting Newtonian fluid down an inclined planar substrate. The substrate is either uniformly hotter (with Marangoni number $M > 0$) or uniformly colder (with $M < 0$) than the surrounding atmosphere. The temperature difference between the substrate and the surrounding atmosphere leads to a surface-tension variation at the free surface of the fluid. The solutions are possible for all inclination angles α when $M > 0$. However, when $M < 0$, there are no possible solutions for this case. Perfectly wetting fluid is significant in production of high quality coating to prevent corrosive condition.

CHAPTER 1

INTRODUCTION

The thesis concerns the unsteady flow of rivulets and flow around dry patches, where the flows are driven either by gravity or surface shear-stress with a strong surface-tension effect. In addition, we also consider the non-isothermal, unidirectional gravity-driven rivulet flows of a Newtonian fluid that perfectly wets an inclined planar substrate. The substrate is either uniformly hotter or uniformly colder than the surrounding atmosphere and the surface tension of the fluid varies linearly with temperature. By using a thin-film approximation or lubrication approximation, the governing mathematical equations describing the fluid flow can be simplified. Accordingly, the first section presents a brief overview of the thin-film flow concept. As the thesis focused primarily on rivulets and dry patches, the overview of these types of flow is presented in Section 1.2, and the classification of fluid is described in Section 1.3. The significance of strong surface-tension effect is outlined in Section 1.4. The following Sections 1.5–1.10 will present our motivation, problem statement, aim and objective, limitation, brief research methodology and finally the thesis outline.

1.1 Overview of Thin-Film Flow

Thin-film flows appear in many diverse settings such as biology, geophysics and industry. As a result, the behaviour of thin-film flows has gained interest among researchers in theoretical and experimental studies. Here, we give examples of the occurrence of the thin film around us which motivate the study of this thesis.

In the biological context, thin films appear almost in every part of the human body. For example, a thin film, known as pre-corneal film, covers the cornea of an eye. This thin film lubricates the surface of the eye concerning the motion of the eyelid for clear vision, to transport waste away and to provide smooth optical surface (Li et al., 2014). In the late 1800s, contact lenses were first designed and used. Thus, the tear film is vitally important to lubricate both the pre-lens and post-lens for the optimal oxygen transport to the cornea during the blink. For instance, Nong and Anderson (2010) designed a model for a pre-lens tear film to deal with the property of the contact lens that affects the behaviour of the thin film. Nowadays, being active is the norm, and people at an early age experience aches especially in the knee and hip for excessive exercises. The diarthrodial joints in the knee and hip, lubricated by synovial fluid (a solution of protein and polysaccharides to reduce friction), can wear away over time (Middleman, 1998). A further example of thin film in the human body is saliva. The main role of saliva is to lubricate the internal surfaces at the oral parts, and thus protect them from injury. Another significant function is saliva enables the swallowing of food-bolus through the oesophagus. The quality of the salivary film coating may vary from one person to another depending on their diet and medical history (Bongaerts et al., 2007; Tripathi, 2011). In the current situation, a novel coronavirus disease, known as COVID-19, could infects the healthy lung causing the lung to become inflamed (Xie and Chen, 2020; Shereen et al., 2020). The fluid lining in the airways of the lung surface is a bilayer thin-film overlays with the periciliary fluid layer and the mucus layer. In the smaller airways, especially, the distribution of this fluid lining is highly affected by surface tension. The fluid prevents the underlying cells from drying and removes inhaled pollutants and bacteria that may threaten the lung. With severe inflammation in



(a)



(b)

Figure 1.1: (a) Brick with guilloché design. (Source picture: <https://www.metmuseum.org/art/collection/search/324618>). (b) A gateway to Emirates Stadium. (Source picture: <https://ibstockbrick.co.uk/news/a-striking-gateway-to-emirates-stadium/>).

the lung, the inflammatory fluids reduced the function of the alveoli in the lung which exchange oxygen and carbon dioxide molecules to and from the bloodstream. Thus resulting in coughing and difficulty in breathing (Jensen, 1997; Craster and Matar, 2000; Grotberg, 2001).

Perhaps the earliest civilization usage of thin film is in glazing process. The pieces of glazed brick panels were restored from diverse archaeological sites and one of them dated to about 890 B.C. from era of Nimrud as shown in Figure 1.1a. The Assyrians invented tin glazing and used it for pottery and brickwork (Gould et al., 2017). Since then, various alternatives glazes have been designed for the purpose of decoration as depicted in Figure 1.1b, to overcome the porosity problem, for energy-saving purpose in building and for durability (Correa and Almanza, 2004; Mohelnikova, 2009; Anderson et al., 2016).

In the modern industry, thin films appear in many areas, such as in motor, food and pharmaceutical industries. Vehicles use thin fluid films to lubricate many component parts such as the engine, brakes and gears (Holmberg et al., 2012). In the food industry,

thin coatings and glazes are used to enhance appearance, add nutritional value and protect against mould (Meza et al., 2015). Furthermore, in pharmaceutical industry, ointments and moisturisers are loosely applied to the skin to prevent it from drying up. Steroid cream is used to relieve itching and inflammation in the treatment of skin conditions such as eczema and psoriasis (Adams et al., 2007).

Before we proceed further, it is necessary to emphasise that the thin film does not represent ‘thin’ in the everyday sense, but it indicates that the length scale of the fluid is much greater than the thickness of the flow. For instance, in a ‘small’ context, thin films of fluid can also be found in everyday life such as oil in a pan, honey on toast, icing on cakes and paint on walls. Meanwhile, in a ‘large’ context, thin flows may be found in geophysical and environmental settings. For example, in gravity currents, landslides, snow avalanches, oil spreading in the sea, lava flows over rocks and sea breezes spreading over land (Griffiths, 2000; Baral et al., 2001; Huppert, 2006; Ancy, 2007). In general, a similar term ‘lubrication flow’ is used to indicate that a thin layer of fluid between the two solid boundaries or free boundaries in motion. This separation of length scales allows the reduction of the governing equations to a simpler form, typically in the aspect ratio. We will further demonstrate this concept in Chapter 3.

1.2 Rivulet and Dry Patch

The continuous flowing fluid on an inclined plane may break up into rivulets, droplets and dry patches as illustrated in Figure 1.2. These formation may arise for a range of factors, for example, due to the wettability of the substrate (Taylor and Michael, 1973; Sharma and Ruckenstein, 1989), the speed of airflows (Hammit et al.,

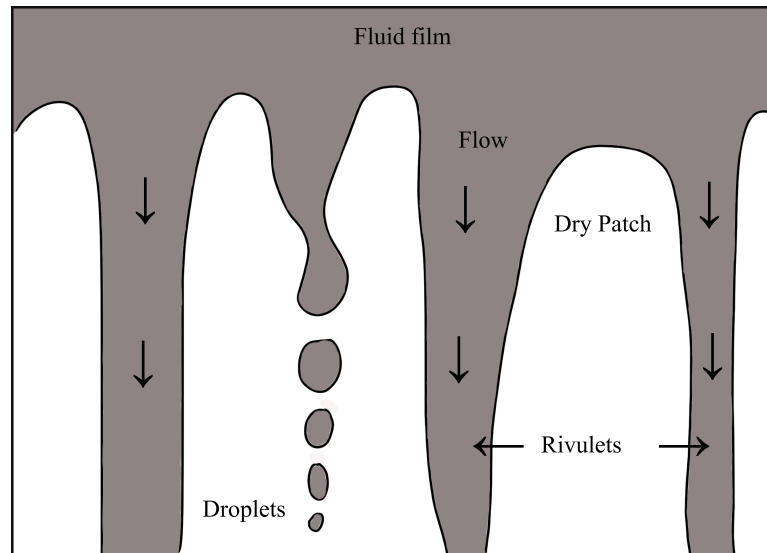


Figure 1.2: Formation of rivulets, dry patches and droplets.

1981), the thickness of the film (Silvi and Dussan V, 1985), the evaporation of the fluid generates critical heat flux on smooth and grooved surface (Sharon and Orell, 1980; Kheshgi and Scriven, 1991; Elbaum and Lipson, 1994; Zaitsev et al., 2007; Anglart, 2015) and the presence of surface contamination (Troian et al., 1989; Marshall and Wang, 2005). Furthermore, the inhomogeneities between the substrate, air trapped within the film, uneven heating and wave motion may set up the formation of the dry patch (Moriarty and Schwartz, 1993).

A rivulet can be defined as a narrow stream and the formation of the non-wetting surface between rivulets is known as a dry patch (Wilson, 1974). A rivulet or referred to as trickle by some researchers shares a curved free surface with the surrounding atmosphere, with contact angles at the three-phase contact lines where the substrate, fluid and the surrounding atmosphere are all in contact (Towell and Rothfeld, 1966; Davis, 1980). A key feature of rivulet flow is that it is long and slender, with the flow predominantly along the rivulet. As mentioned before, rivulets can occur in small-scale flows as well as in large-scale flows. In the non-wetting surface, a dry patch in a fluid

could represent a defect which may grow or shrink due to various disruption of the flow and is controlled by surface tension (Penn et al., 2001; Lv et al., 2018). However, large portions of the surface remain untouched by the fluid, as it clumps together into droplets. Droplets arise from the instability and break up of fluid in the shape of threads and ligaments (Villermaux, 2007). The transition from rivulet to droplets often can be seen obviously at fast-moving subject (Snoeijer et al., 2007). For example, the motion of rainwater on moving vehicles and the spray droplets torn off by the wind at the wave crests in the ocean (Andreas et al., 2001).

In many situations, the formation of the rivulet and dry patch are not preferable (Myers, 1998). This can lead to many kinds of problems such as inefficiency, overheating or corrosion in the dry area. For various applications, from coating processes to micro-patterning, a fundamental understanding of the dry patch is of crucial importance since these processes intend at making a smooth, uniform thin film on any surface. For example, when paint is applied to a surface, it is preferable that the paint does not sag when drying, so that it coats the surface evenly. In the biological context, for instance, the dry patches formed on the cornea can decrease the tear film thickness between blink. The deficiency of this thin film can cause dry eye syndrome which lead to discomfort and the corneal surface damage (Middleman, 1998). In oral health, the reduction of salivary film thickness, may cause a dry mouth condition or xerostomia which can potentially develop difficulties in swallowing, speech, taste sensation and a general deterioration of oral health (Bongaerts et al., 2007).

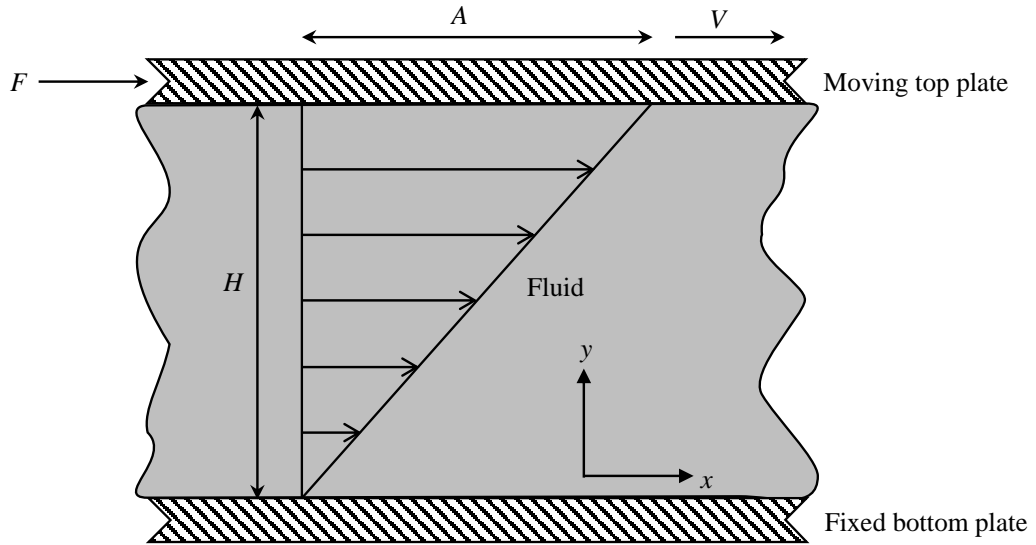


Figure 1.3: Sketch of a simple shearing flow.

1.3 Classification of Fluids

Generally, we can classify fluids as either Newtonian or non-Newtonian fluids, depending on how they behave when deformed. The deformation of fluid is represented by the relationship between shear stress and shear rate as depicted in Figure 1.3. In the simple shearing flow, the fluid is placed in between two horizontal plates. The bottom plate is not moving (fixed), but the top plate is free to move. Let's say we apply the force, F to the top plate in the x -direction. Then, the top plate will move continuously in the x -direction with a velocity, V . This is analogous to the definition of a fluid; when we apply shearing stress to a fluid, it will deform continuously. Hence, the shear stress, τ can be defined as the ratio of the force, F to the surface area, A , which the force is applied upon ($\tau = F/A$). The fluid in contact with the moving top plate moves with the plate velocity, V , meanwhile, the fluid in contact with the bottom stationary plate has zero velocity. Therefore, the fluid velocity at the fluid-solid boundary is the same as the velocity of the solid boundary. This behaviour is known as the no-slip condition. The shear rate, γ can be defined as the gradient of the velocity in the direction at right

angles to the fluid flow, or the ratio of the difference in velocity between two plates to the distance, H between them (Barnes et al., 1989; Munson et al., 2013). As the shearing stress is increased by increasing the force, the shear rate is also increased. Therefore, in general, the shear stress and the shear rate can be related by a simple equation (Munson et al., 2013):

$$\tau = \mu\gamma, \quad (1.1)$$

where μ is the coefficient of the proportionality (fluid apparent viscosity).

1.3.1 Newtonian Fluid

A Newtonian fluid is the fluid whose the shear stress has a directly proportional relationship to the shear rate. This linear relationship between the shear stress and the shear rate of a Newtonian is shown in (1.1) if the coefficient of the proportionality in this relationship is the constant viscosity of the fluid (independent of shear rate). Water and air are good approximation of this type of fluid since no fluid can be described exactly by a Newtonian model (Barnes et al., 1989).

1.3.2 Non-Newtonian Fluid

A non-Newtonian fluid behaves differently from a Newtonian fluid when subjected to shearing force. Unlike the Newtonian fluid, the apparent viscosity, $\mu = \mu(\gamma)$ depends on the shear rate. The non-linear relationship between the shear stress and the shear rate may now be rewritten as

$$\tau = \mu(\gamma)\gamma, \quad (1.2)$$

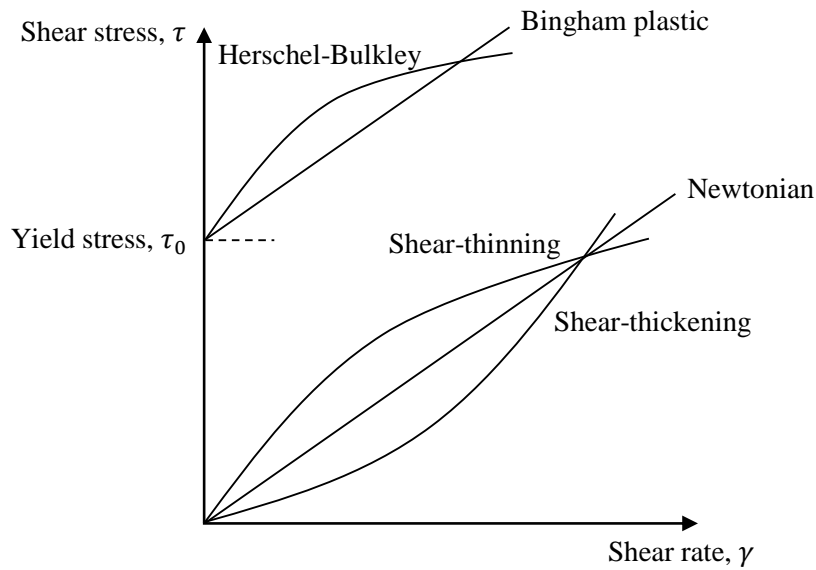


Figure 1.4: The relationship between the shear stress, τ and shear rate, γ for Newtonian and certain generalised Newtonian fluids (time-independent fluids).

where γ is dependent variable of μ . The changes in the apparent viscosity has contributed to many types of non-Newtonian fluids. These fluids may be classified into three main groups, namely the time-independent fluids, the time-dependent fluids and the viscoelastic fluids (Irgens, 2014).

The time-independent fluid is described as a fluid with a single-valued function of shear rate or shear stress. In like manner, the shear rate at a point depends on the corresponding shear stress and vice versa as shown in Figure 1.4. Hence, the time-independent fluids are divided into three subgroups, which are shear-thinning, shear-thickening and viscoplastic fluids. A fluid is said to be shear-thinning (or pseudoplastic) if the apparent viscosity decreases with increasing shear rate. In other words, the fluid is getting less viscous as the increasing shear is given on that fluid. For example, when we shake a bottle of tomato sauce, the sauce gets runnier with the increasing shear, but it eventually returns to its original state when we stop shaking the bottle.

Most of the non-Newtonian fluids such as polymer solutions and biological fluids can be categorized as shear-thinning fluids (Irgens, 2014). The second subgroup is shear-thickening fluid (or dilatant fluid). A fluid is said to be shear-thickening if the apparent viscosity is directly proportional to the shear rate. Unlike shear-thinning fluid, this fluid becomes more viscous as the increasing shear is given on it. For instance, corn-flour solution or custard becomes very sticky when vigorous shear is applied to it and gradually becomes less viscous once the shear is stopped (Munson et al., 2013). Shear-thickening fluid is similar to shear-thinning fluid in a way that it does not have a yield stress. The third subgroup of time-independent fluid is viscoplastic material (Bingham plastic and Herschel-Bulkley) that remains a solid until the shear stress reaches a specific value, known as yield stress, τ_0 , at which point it becomes a fluid and begins to flow (as shown in Figure 1.4). A few fluid models are known for capturing the yield stress with shear-thinning or shear-thickening behaviour, such as the Herschel-Bulkley model and Casson model. On the other hand, the Bingham fluid represents the yield stress with a linear relationship between the shear stress and the shear rate (Irgens, 2014). For instance, when a stress is applied on toothpaste tube, the toothpaste flows out from a tube and remain inside the tube if no stress is applied on it.

The second group of non-Newtonian fluid is the time-dependent fluid. The time-dependent fluid is not a single-valued function since the apparent viscosity also depends on the duration of fluid undergoes shearing. This type of fluids are divided into two subgroups, namely, thixotropic fluids and rheopectic fluids (Irgens, 2014). A fluid is said to be thixotropic fluid when at a constant shear rate and at constant temperature, the shear stress decreases monotonically with respect to time. A thixotropic

fluid is also referred to as time-dependent pseudoplastic fluid. The longer the fluid undergoes shear stress, the lower its viscosity. Examples of thixotropic fluids are yogurt, gelatin gels, drilling fluids, grease, margarine and some polymer melts. In contrast, a fluid is said to be rheopectic fluids or antithixotropic fluid when at a constant shear rate and at constant temperature, the shear stress increases monotonically with respect to time. Antithixotropic fluid is also referred to as time-dependent dilatant fluid. The longer the fluid undergoes shearing stress, the higher its viscosity. Gypsum paste is one of the examples of few real antithixotropic fluids that is used in building materials and in production of tooth models.

The third group is a viscoelastic fluid. It displays a combination of viscous and elastic behaviours. When stress is applied to a viscous material, the material deforms like a liquid. However, an elastic material will stretch when the stress is applied on it and return to the initial configuration when the stress is ceased (Chhabra and Richardson, 2008). This unique characteristic makes the viscoelastic a good absorber and the material is used in mouth guard for sport (Gould et al., 2019).

1.3.3 Power-Law Fluid Model

The non-Newtonian fluids behaviour encountered in most of the applications in our daily life to a complex industrial environment. Hence, several models have been described over the years in the literature to model the three groups of fluid: time-independent fluids, time-dependent fluids and viscoelastic fluids characteristics. The generalised Newtonian model is the simplest type of non-Newtonian fluid model. There are few generalised Newtonian models. For example, power-law model, Cross model,

Ellis model, Spriggs model, Eyring model, Zener-Hollomon model, Carreau model, Casson model, Bingham model, Herschel-Bulkley model and Maxwell model (Barnes et al., 1989; Balmforth et al., 2001; Chhabra and Richardson, 2008; Szeri, 2010; Irgens, 2014).

In this thesis, we shall focus on the simplest generalised Newtonian fluid, namely a power-law fluid which was first proposed by Armand de Waele and Wilhelm Ostwald (Irgens, 2014). In a power-law fluid model, the viscosity is directly proportional to a power of the shear rate given by

$$\mu = \mu(\dot{\gamma}) = \mu_0 \dot{\gamma}^{N-1}, \quad (1.3)$$

where the power-law index, N and the consistency parameter of the fluid, μ_0 are constants. From (1.2), it follows that

$$\tau = \mu_0 \dot{\gamma}^N. \quad (1.4)$$

A power-law fluid model describes a shear-thinning fluid when $N < 1$, a shear-thickening fluid when $N > 1$, and a Newtonian fluid with constant viscosity is recovered when $N = 1$. This model is extensively used in many mathematical modelling because of its simplicity and it may provide analytical solutions. In our study we will focus on Newtonian, shear-thinning and shear-thickening fluids.

1.4 Significance of Strong Surface-Tension Effect

Surface tension is a property of liquids that describes how molecules of the same substance are more likely attracted to each other than molecules of that other substance. The SI unit of surface tension is N/m which is the ratio of force per unit length, specifically, the length of fluid-solid boundary (Potter et al., 2011). Water is a well-known example to illustrate the surface tension. The polar property of water made up from the opposite charges of positive hydrogen and negative oxygen causes attraction between molecules (Starov and Velarde, 2019). For example, when water is deposited on a surface, the water molecules will attract to each other or water molecules surround it. This attraction between water molecules form a strong cohesion or film-like membrane known as surface tension (Docoslis et al., 2000; van Oss, 2003).

We encounter phenomena of surface tension in our daily life. There are few examples where strong surface tension plays a role. The surface of water create a strong cohesion and therefore will give advantage for the water strider to walk on it as depicted in Figure 1.5 (Hu et al., 2003). This situation is not possible for the weak surface tension. Another example is the spherical shape of rain drop (Kumar et al., 2020). The high surface tension of water causes the rain drop to minimize the area, and sphere is the most favourable shape. The balance between the cohesion of the fluid and the fluid adhesion to the surfaces may affect the degree of wetting, the contact angle, and the meniscus shape. Water on hydrophobic surfaces such as lotus plant leaves will display a high contact angle and incredibly difficult to wet. This situation is known as the lotus effect (Zhang et al., 2011).



Figure 1.5: Water striders on surface of water. (Source picture: <https://www.pestwiki.com/water-strider-facts-rid/>)

Huppert (1982a) performed some experiments using three different fluids, namely, glycerine and two types of silicone oil with different viscosity and surface tension flowing down an inclined plane. The instability of the thin film causes the formation of rivulets since the wavelength at the nose of the thin film depends on the surface tension.

All the examples of surface tension above are considered in the environment with gravitational force. Due to gravity, water is pulled downwards to occupy the solid. Fluid will behave differently in the environment with zero gravity or microgravity such as in space where the surface tension effects is dominant (Katsuki et al., 2007). Figure 1.6 shows the droplet and air bubble on a plant in space. The droplet and inside bubble maintain the spherical shape without distortion of gravity. In addition, the droplet stick to the leaf due to molecular adhesion where it would not happen on Earth. Apart of water, for example, fire and crystal also show significant behaviour in the microgravity environment. On Earth, the candle flames resemble teardrops shape, however, they form a uniform oval shape in microgravity where heat does not rise. Astronauts strug-



Figure 1.6: A droplet and air bubble in outer space. (Source picture: https://www.nasa.gov/audience/forstudents/5-8/features/space_gardens_feature.html)

gle to prevent burning in the microgravity environment since the flames can split into flamelets that appear as hemispherical caps. These flamelets move in random motion and will ignite a larger flame if oxygen is reintroduced. Therefore, NASA protocols have specified different approach for astronauts to extinguish fire in space (Wichman et al., 2016). In the microgravity environment onboard the International Space Station (ISS) researchers can develop larger and more well-ordered crystal than on Earth due to lesser distortion from gravity (DeLucas et al., 1989). The conducive environment in ISS has sparked interest in researchers and renowned commercial entities to pursue their research advancement in drug, agriculture and radiation detection (Giulianotti and Low, 2020).

1.5 Motivations of Study

A wide range of applications on various coating processes have motivated the work on this area; from devices such as heat exchangers, trickle-bed reactors and endoscopes tubes to food glazing and skincare creams. In order to maintain the quality of the thin

film, its efficiency and cost-saving, it is crucial to understand the conditions required for the formation of the rivulet and dry patch under various circumstances.

The work in this thesis is motivated by previous researchers in theoretical and numerical simulation. Firstly is the study on a steady flow of dry patch and rivulet on an inclined plane. Wilson et al. (2001) investigated a steady flow of thin film of Newtonian fluid that travels around a slender dry patch by gravity. They found distinct solutions in the case of weak and strong surface-tension effects that involve the dry patch shape and the cross-sectional profile far from the contact line. For the weak surface-tension effect case, the solution predicts a parabolic dry patch increases monotonically far from the contact line. In contrast, for the strong surface-tension effect case, the solution predicts a quartic dry patch with a capillary ridge near the contact line and decays in an oscillatory manner far from it. Later, Wilson et al. (2002) investigated steady rivulet flow of Newtonian and non-Newtonian power-law fluids. They considered flows in the case of weak and strong surface-tension effects. They discovered that the solutions for the flow of gravity-driven or constant-shear-stress-driven are qualitatively similar. They found a unique similarity solution for weak surface-tension effect and one-parameter family of solution for strong surface-tension effect. The solution in weak surface-tension effect corresponds to diverging and shallowing sessile rivulet and converging and deepening rivulet with a single global minimum profile. Meanwhile, the solution in strong surface-tension effect corresponds to diverging and shallowing rivulet with one global maximum, and converging and deepening rivulet with one global maximum or two global maxima.

Second, is the study on the unsteady flow of rivulet and unsteady flow around the

dry patch on an inclined plane by Yatim et al. (2010, 2011, 2012), particularly in a weak surface-tension effect. Yatim et al. (2010) and Yatim et al. (2011) investigated the unsteady gravity-driven flow of a thin slender rivulet of non-Newtonian power-law fluids and special case for Newtonian fluid, respectively. Their solution predicts that a rivulet with a fixed nose has either a single-humped or double-humped cross-sectional profile that widens and thickens (for a sessile rivulet) or narrows and thins (for a pendent rivulet) with time. Nevertheless, they found no solution for dry patches. A similar approach used by Yatim et al. (2012) for constant shear stress drives the flow on the free surface. In this study, there is only one physically realisable solution of rivulet representing the single-humped cross-sectional profile. The similarity solution describing the flow around dry patch is obtained which is absent in the previous studies of Yatim et al. (2010) and Yatim et al. (2011).

The recent studies by Abas and Yatim (2017) and Abas (2017) used the travelling-wave similarity solution with the effect of strong surface tension. The solution predicts that the quartic shape of the rivulet maintain its cross-sectional profile height but change its width as time elapse when the rivulet velocity up or down the substrate. The solutions of the rivulet always has a single global maximum at $y = 0$, and depend on free parameters at the boundary condition and the rivulet velocity. Abas (2017) found the dry patches concave upward for different cross-sectional profiles; increase monotonically and decay in an oscillatory manner far from the contact line. The significant difference between our problem from Abas and Yatim (2017) and Abas (2017) is the type of the similarity solution; our similarity solutions of the rivulet and dry patch do not depend on the travelling-wave velocity and have a fixed nose at origin, O as

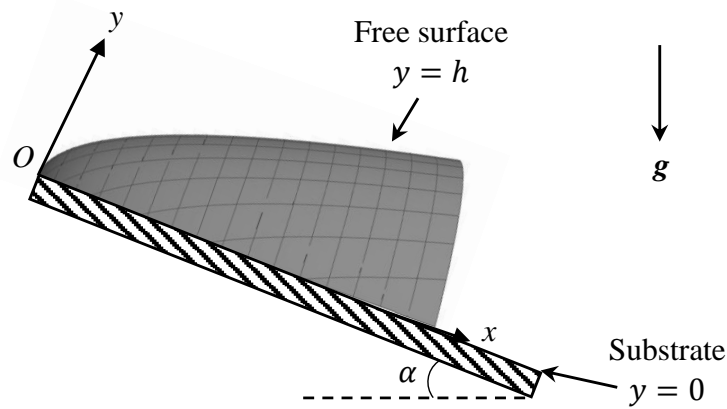


Figure 1.7: Rivulet flows on an inclined plane.

depicted in Figure 1.7 while flowing down the substrate with an inclination angle α .

Motivated by these previous work, we noticed that the classification of fluid flows and surface-tension effect are important in finding the similarity solutions of rivulets and dry patch on an inclined plane. Therefore, in this thesis, we are interested in investigating the strong surface-tension effect on the Newtonian and non-Newtonian power-law fluids of rivulet and dry patch both driven by gravity and constant surface shear stress. The work are described in Chapters 4-7.

In many situations, the thermal effect is significant to the fluid flow. Despite its importance, there has been surprisingly little research on non-isothermal rivulet flow to date. For the non-isothermal flow, the energy balance equation requires boundary conditions that may consist of fixed temperature at the boundaries or they may be more complicated and incorporate thermal effect such as heat transfer at the boundaries (Leslie et al., 2011). Holland et al. (2001) investigated unidirectional steady rivulet of Newtonian fluid flow on a uniformly heated or cooled substrate. The surface tension varies linearly with temperature and cause the fluid flow differently from the isother-

mal problem. Next, Wilson and Duffy (2003) and Duffy and Wilson (2003) considered the effect of thermoviscosity on a rivulet flowing down a heated or cooled slowly varying substrate for three different viscosity models, namely a linear, an exponential and an Eyring model in the cases of both non-perfectly wetting and perfectly wetting. Duffy and Wilson (2003) have performed further studies of the flow of a perfectly wetting fluid rivulet down a slowly varying substrate for the case when the viscosity is temperature-dependent and the substrate is uniformly heated or cooled. Perfectly wetting fluid is a fluid that completely wets the substrate and has zero contact angle between the fluid and the substrate. Duffy and Wilson (2003) found that a perfectly wetting sessile rivulet (rivulet on top of the substrate) is not possible, but a perfectly wetting pendent rivulet (rivulet underside of the substrate) is possible. All of these work invoke a boundary condition involving heat transfer at a free surface with Newton's law of cooling. Since the findings of non-perfectly wetting and perfectly wetting fluid for the case of thermoviscosity have significant differences, we would like to investigate in the case of thermocapillary with perfectly wetting Newtonian fluid. The work on this problem is discussed in Chapter 8.

1.6 Problem Statement

In the literature, many scholars have successfully obtained the similarity solution for various thin-film problems encountered in either steady or unsteady fluid flows. The importance of an unsteady flow property is to predict the evolution of the thin film draining down an inclined plane as time goes by with different types of physical mechanisms such as gravity or constant shear stress that driving the flow (Wilson et al., 2001, 2002). Due to this factor, the thin film may coat the substrate (as a rivulet) or

may not coat the substrate (as a dry patch).

Previously, researchers took a simple geometry of problem, for instance, a flow on a horizontal substrate to study the flow of a thin film theoretically and experimentally (Huppert, 1982b). Nowadays, with advanced technology, we can study and verify the flow of a thin film in various geometry of the substrate to imitate the real-world application. In this thesis, we focus on the flow of a thin film draining down an inclined plane which can be a good start-up for a more complicated geometry. When the plane is vertical in the steady flow, the effect of surface tension has an impressive impact that deserves attention (Duffy and Moffatt, 1997). This effect can be incorporated conveniently into the governing equation by assuming it is stronger than flow driven by gravity or constant shear stress (Wilson et al., 2001, 2002; Abas and Yatim, 2017). Usually, the presence of the surface tension results in a non-linear and of the fourth-order parabolic equation for the film thickness (Myers, 1998). In the vicinity of the front of thin film, the large curvature of the free surface is influenced by the surface tension (Perazzo and Gratton, 2003). As a result, the capillary ridge with monotonically increasing or oscillatory decaying can be observed (Holland et al., 2002).

Numerous studies incorporated with the surface tension also showed that the stability of the thin film strongly depends on it (Ponter et al., 1967; Wilson, 1974). However, a comparison study with experiment tends to be challenging with strong surface-tension effect. The changes in surface tension at liquid-gas interphase or Marangoni effect is due to solute concentration, surfactant concentration and temperature along the interface. Specifically, when the surface tension varies with the concentration, the Marangoni effect is known as the solutocapillary effect, while, when the surface

tension varies with the temperature, the Marangoni effect is known as the thermocapillary effect (Nakajima et al., 2003; Mizev et al., 2013; Karapetsas et al., 2014). It is also found that the contact angle between the fluid and the substrate with temperature dependent viscosity (thermoviscosity) affected the behaviour of the unidirectional gravity-driven of a thin rivulet of a Newtonian fluid (Duffy and Wilson, 2003). Also, few analytical results are known for problem when surface tension is taking into consideration and hence some researchers choose to neglect surface tension (Momoniat et al., 2009).

The study of similarity solution for the unsteady three-dimensional flow of rivulet and flow around a dry patch with the strong surface-tension effect is yet still lacking in theoretical and this is a gap that needs to be dealt with. There are few researchers have addressed the problem of the steady unidirectional gravity-driven draining of a thin rivulet, in particular, when the surface tension of the fluid varies linearly with temperature. However, the characteristic of rivulet flows with zero contact angle (in the case of perfectly wetting fluid) have not been dealt in depth. This research will lead to a new piece of information in recognising and describing the behaviour of an unsteady fluid on an inclined plane in the case of strong surface-tension effect.

1.7 Aim and Objectives of Study

This thesis aims to analyse five problems of three-dimensional thin-film flows of rivulet and flows around dry patch on an inclined plane. In the first four problems, we seek similarity solutions for unsteady three-dimensional thin-film flow of a slender rivulet and around a slender dry patch on an inclined plane, for both gravity-driven and

constant-shear-stress-driven flows in the case of strong surface-tension effects. The Newtonian and non-Newtonian power-law fluids shall be considered. While for the final problem, we seek solution for steady unidirectional gravity-driven rivulet flow of perfectly Newtonian fluid with thermocapillary effects. Therefore, the objectives of this thesis are:

1. to construct mathematical model by using the equations of motion and continuity equation based on the lubrication theory,
2. to carry out the mathematical formulations with the appropriate boundary conditions in finding the pressure and velocity of the flow,
3. to seek the similarity solutions of the appropriate governing equations in predicting the height and width of the flows, and
4. to obtain the numerical solutions of the ordinary differential equations for thin-film flows.

1.8 Limitation of Study

This research has a few limitations. The four problems from Chapters 4 to 7 presented in this thesis are only limited to the unsteady three-dimensional thin-film flow of Newtonian and non-Newtonian power-law fluids on an inclined plane which is formulated using certain type of similarity solution and solved using the shooting method. The solutions shown in this study are also restricted to certain values of the power-law index, N of non-Newtonian fluid from previous studies. The problem in Chapter 8 is limited to steady three-dimensional thin-film flow of perfectly wetting Newtonian fluid

with thermocapillary effect. The governing ordinary differential equation is solved by using `NDSolve` built-in function with prescribed volume flux. Furthermore, this study is based on the numerical results and simulations since no experimental work is carried out. Despite this, we believe our work could be the basis for others to explore in the future work as suggested in Chapter 9.

1.9 Research Methodology

The mathematical model of each problem is designed for the unsteady and steady three-dimensional thin-film flow down an inclined plane driven by either gravity or constant shear stress. The problem formulation is constructed with the continuity equation and equations of motion that are derived using the lubrication theory. The mathematical formulations are carried out with the appropriate boundary conditions and kinematic conditions to obtain the governing partial differential equation.

The governing partial differential equation is reduced into the ordinary differential equation using the similarity transformation (Chapter 4-Chapter 7). Then, the ordinary differential equation is non-dimensionalised with appropriate variables.

The ordinary differential equation are solved numerically if there are no closed-form solutions. To obtain the solution, the ordinary differential equation with appropriate boundary conditions is treated as an initial value problem. It is solved by using a shooting method in *Mathematica* 12 with `NDSolve` built-in function as presented in Chapters 4 to 8.

The flow chart for the research methodology is shown in Figure 1.8 for Chapters 4-

7. The research methodology for Chapter 8 does not require similarity solution and the non-dimensionalisation is introduced earlier before obtaining the governing ordinary differential equation.

1.10 Thesis Outline

In this thesis, we analyse the flow behaviour of rivulets and flow around dry patches on an inclined plane. In Chapter 1, a brief overview of thin-film flow, rivulets and dry patches, classification of fluids and the significance of a flow with strong surface-tension effect are given. Motivation of study, problem statement, aim and objectives of study, its limitation and research methodology are also presented in this chapter. In Chapter 2, a brief history of Navier-Stokes equation, literature reviews of relevant studies on thin-film fluid flows driven by external forces and other forces such as by centrifugal forces, thermal effects, intermolecular forces and surfactant are discussed. In Chapter 3, the formulation of governing equations and the methods that will be used in the thesis are derived. From Chapters 4 to 8, the details of the five problems concerned in this thesis are discussed.

In Chapter 4, we investigated the unsteady three-dimensional gravity-driven flow of thin slender rivulet of Newtonian and non-Newtonian power-law fluids on an inclined plane with strong surface-tension effect. Then, in Chapter 5, we considered the same flow of thin film of Newtonian and non-Newtonian fluids around a slender dry patch. In Chapters 6 and 7, we extended our work in Chapters 4 and 5 to consider the rivulet flow and flow around a dry patch which are driven by constant surface shear stress. We seek similarity solutions of these problems. The behaviour of the flows are discussed